Above Room Temperature Multiferroic and Magneto-electric Properties of (1-Φ) PZTFT-Φ CZFMO Particulate Composites

Krishnamayee Bhoi[1, 2], Dhiren K Pradhan[3*], Hari Sankar Mohanty[a1,2], W.L.N.C. Liyanage[4], Alok Barik[5], M. M. Rahaman[6], S. N. Babu[g7], Dustin A. Gilbert[3,4], P. D. Rack[3] and Dillip K. Pradhan[8]*

[1]Department of Basic Science and Humanities, GIET University, Gunupur, Odisha-765022, India

[2] Department of Physics, School of Sciences, GIET University, Gunupur, Odisha-765022, India

[3]Department of Materials Science and Engineering, University of Tennessee, Knoxville, Tennessee 37996, USA.
[4]Department of Physics & Astronomy, University of Tennessee, Knoxville, Tennessee 37996, USA

[5]Department of Physics, Madanapalle Institute of Technology & Science, Madanapalle-517235, Andhrapradesh, India

[6]Department of Material Science and Engineering University of Rajsahi, Rajsahi-6205, Bangladesh.

[7]Materials Research Laboratory, Department of Physics, Osmania University, Hyderabad 500007, India

[8]Departments of Physics and Astronomy, National Institute of Technology, Rourkela, Odisha 769008, India

Corresponding Author:

Email: dhirenkumarp@gmail.com, dillip.pradhan79@gmail.com

ABSTRACT

Magnetoelectric (ME) composites of suitable ferroelectric and magnetic materials can display elevated magnetic and ferroelectric operational temperatures, along with substantial ME coupling, compared to conventional single-phase multiferroics. Herein, we describe the synthesis of (1-Φ) PZTFT-Φ CZFMO, Φ = 0.1, 0.2, 0.3 (PZTFT: $[0.6(PbZr_{0.53}Ti_{0.47}O_3)$-$0.4(PbFe_{0.5}Ta_{0.5})O_3]$ CZFMO: $Co_{0.6}Zn_{0.4}Fe_{1.7}Mn_{0.3}O_4$)] particulate (0-3) composites and report on the magnetic as well as ferroelectric phase transitions and magneto-electric coupling. The phase formation and the induced strain in these composites are investigated via Raman spectroscopy. A large bifurcation of the zero field cooled-field cooled magnetization curves confirms the highly anisotropic behavior of the composites. These curves also identify spin glass behavior in the CZFMO phase at ≈230 K. The magnetic phase transition of the composite (Φ = 0.2) is reported to be ≈532 (±10) K. The temperature dependent dielectric data displays the ferroelectric phase transitions from the PZTFT

phase and the broad relaxation peak from the CZFMO phase. The quadratic relationship between the magneto-capacitance and the magnetization confirms the existence of biquadratic magneto-electric coupling in the systems. The collective results are consistent with the presence of a direct magneto-electric effect in the composites i.e. by the application of magnetic field, the magnetic phase is strained, and this induced strain is responsible for changes of ferroelectric order parameter in the piezoelectric phase. This attribute makes the current composite structure a promising candidate for multiferroic data storage and processing technologies.

I. INTRODUCTION

There is tremendous research interest in magneto-electric multiferroic materials due to the co-existence of more than one ferroic orders along with the cross coupling between them.[1-3] The magneto-electric effect i.e. a change in electronic polarization by the application of a magnetic field or a change in magnetization under the application of an electric field, adds additional functionalities in these classes of materials that can be leveraged in the design of new electronic and spintronic devices.[1,2] The figure of merit in magneto-electric systems is the magneto-electric coupling coefficient, which encodes the cross coupling strength between ferroelectric and magnetic ordering. Multiferroics are broadly categorized into two classes based on whether the magneto-electric coupling is intrinsic to the material, e.g. single phase, and or if the system is a composite.[2,3] The single phase and composite multiferroics differ in terms of symmetry, structure, design, and other physical and chemical perspective.[1,3] There are few single phase multiferroics, since the transition metals in most ferroelectrics have empty d-shells, while d-shell occupancy is generally necessary for magnetic ordering, resulting in a mutual exclusion of multiferroic coexistence.[3] However, single phase multiferroics are available by the consequence of several phenomena such as combination of perovskites with d^0 and d^n ions, ferroelectricity due to lone

pair effect, ferroelectricity due to charge ordering, geometric driven ferroelectricity and ferroelectricity due to spin driven mechanism (symmetric exchange striction, asymmetric spin exchange interaction, the spin dependent p-d hybridization mechanism).[1,3] However, single phase multiferroics are rare and they show weak magneto-electric coupling behavior at room temperature (RT). Multiferroic composites present an alternative which can achieve strong magneto-electric behavior at and above RT. The magneto-electric coupling in composites can be mediated via multiple ways including strain, charge transfer, and spin exchange.[4,5] Magneto-electric coupling through interfacial strain, e.g. coupling piezoelectric and magnetostrictive phases, is the most studied multiferroic composite. When strain mediation is operative, several factors can be optimized in order to obtain a strong magneto-electric effect, namely: (i) increasing the strain response from the piezoelectric phase and magnetostrictive phase i.e. selection of high piezoelectric and magnetostrictive coefficient of the respective phases (ii) optimizing the strain transfer between the constituent phases through strong interfacial coupling.[4,6] Most of the common connectivity in the composites are particulate (0-3 type), laminate (2-2 type) and rod (1-3 type) composites.[4] However, particulate composites are easy to fabricate and show an isotropic response.[6]

In order to achieve strong magneto-electric coefficient at room temperature in the composites, the selection of the materials plays an important role. For strain mediated ME composite, the ferroelectric phase is chosen on the basis of material with morphotropic phase boundary (MPB) composition of ferroelectric solid solutions, that are capable of showing strong ferroelectric/piezoelectric properties, low dielectric loss, high dielectric constant, good electrical poling strength etc.[7] During the fabrication of composite, the piezoelectric strain constant, piezoelectric voltage constant, mechanical quality factor, curie temperature (T_C), remnant

polarization for the ferroelectric phase are also taken in to consideration.[7] For the magnetic phase, the material with good magnetization, magnetic permeability, remanent magnetization, coercivity, piezomagnetic coefficient, magnetostrictive coefficient, good resistivity are desirable.[7] The Curie and Neel temperature should also be above room temperature. In order to fabricate the 0-3 type particulate composites, we have considered PZTFT as the matrix and CZFMO as the dispersive phase. PZTFT is a solid solution of PZT ($PbZr_{0.53}Ti_{0.47}O_3$) and PFT ($PbFe_{0.5}Ta_{0.5}O_3$) and shows multiferroic behavior around room temperature (RT).[8,9] PZTFT undergoes sequential phase transitions cubic to tetragonal, tetragonal to orthorhombic and orthorhombic to rhombohedral with decrease in temperature.[9] This material shows good magnetic and ferroelectric properties with low leakage current at room temperature.[8,9] PZTFT exhibits dielectric constant of ~6000 at 475 K and saturated polarization of 25 $\mu C/cm^2$ at room temperature.[9] It shows good ferroelectric and ferromagnetic properties, magneto-electric behaviors at room temperature. PZTFT is reported to be the lowest loss room temperature multiferroics.[9] The high dielectric constant and good ferroelectric response of PZTFT is also expected to sustain high electric field for electrical poling. Due to the above mention fascinating properties, PZTFT is taken as matrix for the fabrication of magneto-electric composite. Among ferrites, $CoFe_2O_4$(CFO) shows large magnetostriction coefficient of 150-250 ppm.[10] But the disadvantage in CFO is associated with large co-ercivity and magnetostriction coefficient. It has been reported that, the substitution of Mn and Zn in CFO ($CoFe_{1.7}Mn_{0.3}O_4$ and $Co_{0.6}Zn_{0.4}Fe_2O_4$) reduce the coercivity and anisotropy in CFO by keeping the magnetostriction coefficient comparable to that of CFO.[11] The optimized composition $Co_{0.6}Zn_{0.4}Fe_{1.7}Mn_{0.3}O_4$ (CZFMO) CZFMO is reported to exhibit the sizeable magnetostrictive coefficient (λ_{11} = -20 ppm, λ_{12} = 10 ppm), comparable magnetization to that of CFO along with the high electrical resistivity ($10^8 \Omega$ cm),[11]. The high electrical resistance is necessary to minimize

leakage current in the composite structure. Besides, the PZT-CZFMO based composites show enhanced magnetoelectric behavior compared to the composite of undoped CFO.[10] These qualities of CZFMO make it ideal for magneto-strictive phase of the proposed composite. The hybrid synthesis technique is adopted in this study and is expected to improve the homogeneity of the two phases, reducing the chainlike connections which tend to occur within the magnetic phase.[12] This technique also decreases the chances of pore trapping at the interface between the constituent phases, improving the coupling.[13,14]

Here, we report the ferroelectric and magnetic phase transition behavior of the (1-Φ) PZTFT-Φ CZFMO (Φ = 0.1, 0.2, 0.3) composites. The effect of CZFMO phase on the ferroelectric phase transitions in the PZTFT phase have been investigated. The magnetic phase transitions in these composites are studied from the temperature dependent magnetization (M-T) data. Raman spectroscopy and magneto-electric properties of these composites at RT are analyzed. Compositions of Φ = 0.1, 0.2, 0.3 are considered here and an ideal magnetoelectric structure is identified based on an optimization of their dielectric, piezoelectric, ferroelectric, magnetic properties, and magneto-electric coupling.[15]

II. EXPERIMENTAL

The (1-Φ) PZTFT- ΦCZFMO (Φ = 0.1, 0.2, 0.3) are prepared by a hybrid synthesis technique.[13] The constituent PZTFT and CZFMO phases are prepared using a solid state synthesis method and sol-gel method, respectively. To synthesize PZTFT, stoichiometric proportion of PbO, Fe_2O_3, ZrO_2, Ta_2O_5, TiO_2 powders are mixed; 10 wt. % of extra PbO is added to the PZT- PFT phase while preparing PZTFT to compensate the lead loss. The raw ingredients for PZTFT phase are ground for several hours in acetone medium then calcined at an optimized temperature of 1123 K

for 10 hrs. The CZFMO phase is prepared using $(CH_3COO)_2Co•4H_2O$, $Fe(NO_3)_3•9H_2O$, $Zn(NO_3)_2•6H_2O$, and $Mn(CH_3COO)_2•4H_2O$ precursors following a sol-gel method. The detailed synthesis procedure is reported elsewhere.[6] The (1-Φ) PZTFT-ΦCZFMO (Φ = 0.1, 0.2, 0.3) composites are prepared from the calcined powder of PZTFT and CZFMO at the desired weight percentages. The calcined powder of PZTFT and CZFMO are ground in air medium followed by mixing several hours in acetone medium. The (1-Φ) PZTFT Φ CZFMO (Φ=0.1, 0.2, 0.3) pellets are made and sintered at an optimize temperature of 1523 K for 4 hrs.

Raman spectra of the composites are recorded using a Raman spectrometer (WITEC alpha 300R, wavelength is 532 nm and laser power is 5 mW). The magnetization versus magnetic field (M-H) and magnetization versus temperature (M-T) measurements of the composites are carried out using a DynaCool physical properties measurement system (PPMS) from Quantum Design. The temperature and frequency dependent dielectric properties are measured using HIOKI IM3570 impedance analyzer. The RT magneto-dielectric properties of the composites are collected using an impedance analyzer (Wayne Kerr 6500B) coupled with an electromagnet (GMW-5403). The magneto-electric coefficient for PZTFT-CZFMO is measured with the help of magnetoelectric set up using dynamic method. Firstly, the sample under investigation is placed between the pole pieces of DC electromagnet. The AC Helmholtz coils (130 turns mounted on the DC magnetic pole pieces) are excited by 1.008 kHz low amplitude high frequency signal using dual phase lock-in amplifier.In order to amplify the signal current, further a power amplifier is used to drive the Helmholtz coil. The generated AC magnetic field is estimated by measuring the current passing through the Helmholtz coil with the help of Keithley 196 DMM. Now, the magnetoelectric coefficient is calculated by recording the induced voltage across the sample when an AC magnetic field and DC bias are applied to the sample. In the present work, the ME coefficient with DC

magnetic field (0 to 5 kOe) is performed with applied AC field of 1 Oe (1.008 kHz) keeping the AC and DC magnetic field along the thickness of the sample.[6]

III. RESULTS AND DISCUSSION

A. Raman Study

Raman spectroscopy is used to measure the lattice vibrations, which are shifted by structural modifications in the crystal, with sensitivity to doping at crystallographic equivalent sites of a unit cell. Thus, the composition-dependent Raman scattering spectra of the PZTFT-CZFMO composites have been investigated in the range of 50-1000 cm^{-1} using the damped harmonic oscillator (DHO) model to apprehend the formation of two-phase composites and the effects of composition on its structure as well as CZFMO on PZTFT matrix.[16, 17] The intensity of the measured scattering at a given frequency, $I(w)$, can be described in this model as:

$$I(\omega) = [n(\omega)+1] \sum_i \frac{A_i \Gamma_i \omega_i^2 \omega}{\left(\omega^2-\omega_i^2\right)^2+\omega^2\Gamma_i^2} \quad \ldots\ldots\ldots\ldots\ldots\ldots (1)$$

where, $n(\omega) = \frac{1}{\exp\left(\frac{\hbar\omega}{k_B T}\right)-1}$ is the Bose-Einstein population factor, k_B is the Boltzmann constant, $\hbar$ is the Dirac constant. The amplitude, damping constant, and frequency of the i^{th} Raman active optic mode are denoted as A_i, Γ_i, and ω_i, respectively.

The Raman scattering spectrum of the PZTFT ceramic, fitted with Eq. (1), is displayed in Figure 1(a).

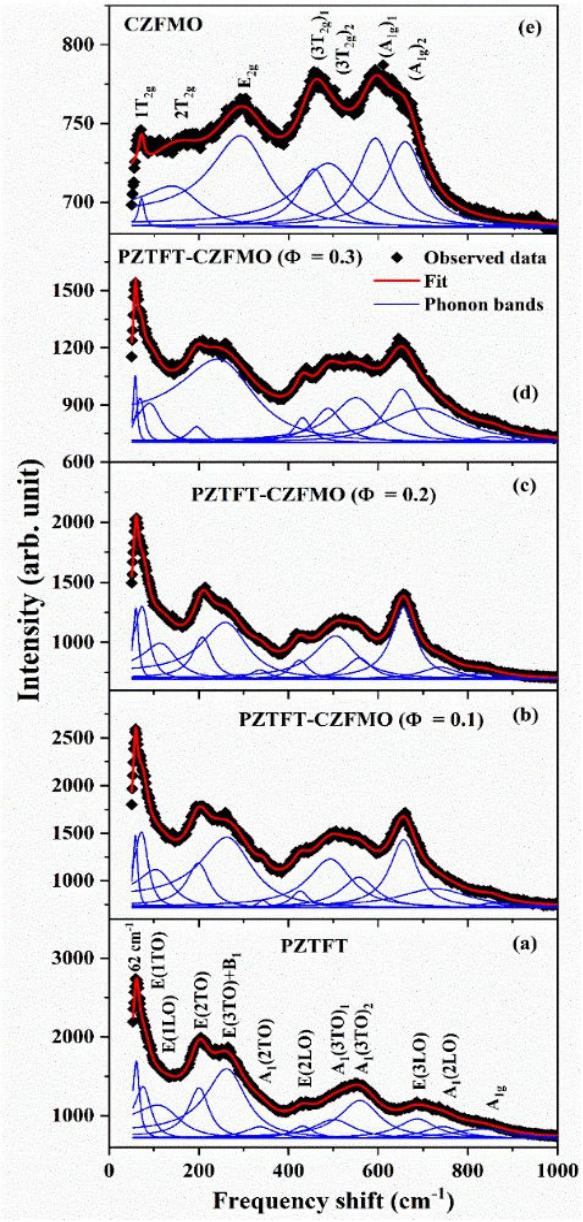

FIGURE 1 Room temperature fitted Raman scattering spectra of (a) PZTFT (Φ = 0.0), (b) PZTFT-CZFMO (Φ = 0.1), (c) PZTFT-CZFMO (Φ = 0.2), (d) PZTFT-CZFMO (Φ = 0.3), and (e) CZFMO (Φ = 1.0) of (1-Φ)PZTFT-ΦCZFMO composite. The spectra were fitted by the Equation (1).

A series of broad overlapping bands is observed in the Raman spectrum of the PZTFT, which is typical of samples with a tetragonal phase.[9] The optical modes in the cubic phase of $PbTiO_3$ with $Pm\bar{3}m$ symmetry is represented as the $3T_{1u}+T_{2u}$ irreducible presentations. The triply degenerate T_{2u} mode is both Raman and infrared inactive, whereas the three triply degenerate T_{1u} modes are infrared active. All of the optical modes turn into Raman-active in the ferroelectric tetragonal phase with *P4mm* symmetry. In the tetragonal phase, the T_{2u} mode splits into B_1+E modes, and each of the T_{1u} modes splits into A_1+E modes. Thus, the optical Raman modes in the tetragonal phase with *P4mm* symmetry transform as $3A_1+4E+B_1$. In ceramics, the mode symmetry assignments are not possible from the Raman scattering spectra directly, thus, we pursue our mode symmetry assignments as in PZT35 single crystals.[18] As can be seen in Figure 1(a), the Raman spectrum of the PZTFT ceramic consists of mainly E(1TO)≈82 cm^{-1}, E(1LO)≈137 cm^{-1}, E(2TO)≈204 cm^{-1}, [E(3TO)+B_1] doublet≈272 cm^{-1}, A_1(2TO)≈340 cm^{-1}, E(2LO)≈433 cm^{-1}, A_1(3TO)≈550 cm^{-1}, E(3LO)≈690 cm^{-1}, A_1(2LO)≈746 cm^{-1}, and A_{1g}≈836 cm^{-1} modes in the frequency range of 50-1000 cm^{-1}. Note that the A_1(3TO) mode splits into two modes marked as $A_1(3TO)_1$≈506 cm^{-1} and $A_1(3TO)_1$≈564 cm^{-1} indicating the existence of different local order regions in the PZTFT ceramic.[18-20] The E(2TO) and E(3TO)+B_1 modes are associated with a rotation of the BO_6 octahedra, while A_1(2LO) and $A_1(TO_3)$ modes correspond to B-O stretching and O-B-O bending of oxygen octahedra, respectively.[21] An octahedral breathing A_{1g} mode is found in the high-frequency range of ≈834 cm^{-1} [Figure 1(a)]. For a simple perovskite, the symmetric A_{1g} breathing mode, which is Raman inactive, appears in this region and does not result in a change in polarization.[22] When ions with different radii are in the center of the octahedra they produce asymmetry in the breathing-like mode and this A_{1g} mode becomes Raman active.[21] Thus, the presence of the A_{1g} mode may imply the occupancy of $Zr^{4+}/Ti^{4+}/Fe^{3+}$ in the BO_6 octahedra.

It is notable that the A_{1g} mode near 834 cm^{-1} was not found in the PZT single crystal/ceramics/thin films. [18, 24, 25] Hence, another possibility is that the A_{1g} mode may be due to the magnetic nature of the PZTFT ceramic in addition to ferroelectricity, which is induced by the Fe^{3+} ions at the B-site octahedral. The spontaneous magnetostriction associated with displacements of cations may stem from magnetic ordering. The lattice distortion caused by the displacements of cations leads to the appearance of new vibrational modes in the PZTFT ceramics. Note that a sharp phonon mode appears at about 61 cm^{-1} [Figure 1(a)], which may correspond to $B_2(TO_1)$ mode of the orthorhombic phase with *Pmm2* symmetry of the PZTFT ceramics. The temperature-dependent dielectric properties also support the orthorhombic phase at RT of the PZTFT ceramics in this study. According to group theory analysis, the cubic phase with $Fd-3m$ symmetry of the cobalt ferrite $CoFe_2O_4$ (CFO) has A_{1g}(R), E_g(R), T_{1g}, $3T_{2g}$(R), $2A_{2u}$, $2E_u$, $4T_{1u}$ (IR) and $2T_{2u}$ phonon modes. [26, 27] Among them, A_{1g}, E_g, and $3T_{2g}$ are Raman active modes. The Raman modes assignment of the CZFMO based on these predictions is shown in Figure 1(e). It is seen from Figure 1(e) that the Raman spectrum of the CZFMO comprise $1T_{2g}$≈72 cm^{-1}, $2T_{2g}$≈177 cm^{-1}, E_g≈313 cm^{-1}, $3T_{2g}$≈463 cm^{-1}, and A_{1g}≈600 cm^{-1}. The present results are similar to those observed in CZFMO ferrite. [26,28] In this study, the observed Raman modes above 100 cm^{-1} of the CZFMO also match with undoped CFO at 210, 311, 470, 577, 624, and 694 cm^{-1}.[29] The decrease of the observed Raman modes in comparison with that of the undoped one indicates the incorporation of Mn and Zn into the CFO lattice. The Raman modes in the range of 460 cm^{-1} - 640 cm^{-1} are associated with octahedral *B*-site in AB_2O_4-type ferrites, whereas the Raman modes around 660 cm^{-1} -720 cm^{-1} are related to tetrahedral A-site. [10, 30] In octahedral *B*-site, the bending of oxygen octahedra towards the metals may lead to the T_{2g} and E_g modes below 600 cm^{-1}. [26, 10] The A_{1g} mode in the high-frequency region expresses the metal-oxygen bond symmetric stretching in tetrahedral

A-site. [10] Note that the A_{1g} and $3T_{2g}$ modes split into two modes at about 597 cm^{-1} and 664 cm^{-1}, and 460 cm^{-1} and 500 cm^{-1}, respectively. The Raman mode splitting of the CZFMO ceramic may be due to the short-range ordering of cations at the A and B sites which lowers/breaks the symmetry. [30]

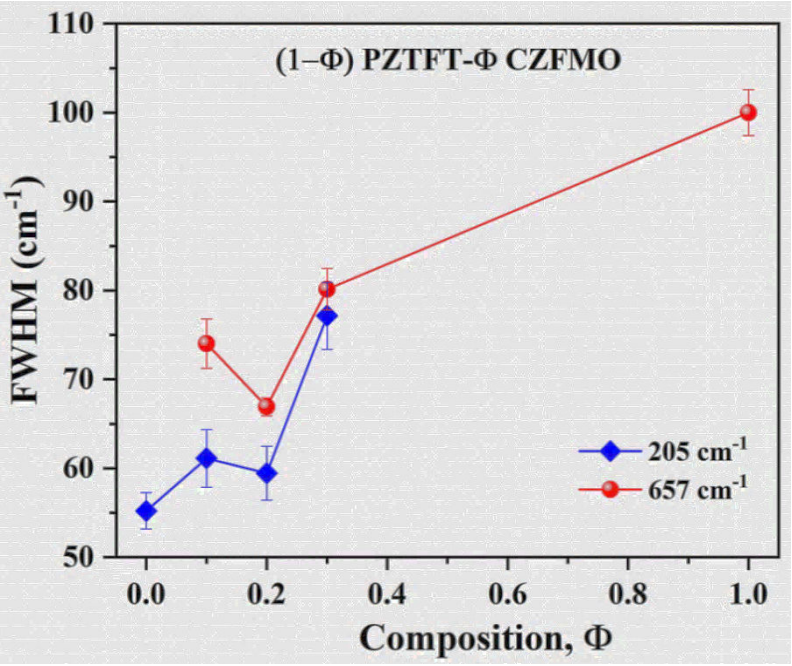

FIGURE 2 The full width at half maximum (FWHM) of the modes near 205 and 657 cm^{-1} of the PZTFT-CZFMO composite as a function of composition.

It is notable that the A_{1g} mode near 834 cm^{-1} was not found in the PZT single crystal/ceramics/thin films. [18, 24, 25] Hence, another possibility is that the A_{1g} mode may be due to the magnetic nature of the PZTFT ceramic in addition to ferroelectricity, which is induced by the Fe^{3+} ions at the B-site octahedral. The spontaneous magnetostriction associated with displacements of cations may stem from magnetic ordering. The lattice distortion caused by the displacements of cations leads to the appearance of new vibrational modes in the PZTFT ceramics. Note that a sharp phonon mode appears at about 61 cm^{-1} [Figure 1(a)], which may correspond to $B_2(TO_1)$ mode of the

orthorhombic phase with *Pmm2* symmetry of the PZTFT ceramics. The temperature-dependent dielectric properties also support the orthorhombic phase at RT of the PZTFT ceramics in this study. The composition-dependent Raman spectra of the PZTFT-CZFMO (Φ = 0.1, 0.2, 0.3) composite recorded at RT are displayed in Figure 1(b,c,d), respectively.

The fitted Raman spectra assess the formation of composite PZTFT-CZFMO by observing Raman modes corresponding to both CZFMO and PZTFT. The E_{2g} modes corresponding to the CZFMO phase merge with $E(3TO)+B_1$ mode corresponding to the PZTFT phase, resulting in the broadening of the mode of the composite. However, the Raman spectra of the composite are similar to the end member of PZTFT. This finding suggests that the properties of the composite may be dominated by the PZTFT ceramics. The absence of any chemical reaction between the constituent phases is confirmed by noting the absence of additional peaks in the Raman spectra of the composite samples. This result is also supported by X-ray diffraction (XRD) and field emission scanning electron microscopy (FESEM) results as per our previous report. [15] The Raman mode of the composite near 205 cm^{-1} corresponds to the E(2TO) mode of the PZTFT, whereas the mode near 657 cm^{-1} stems from the $(A_{1g})_1$ mode of the CZFMO. In the composite, the significant strain due to lattice distortion is observed by the change in damping constants of the phonon modes near 205 cm^{-1} and 657 cm^{-1} in comparison with the end members. Note that the damping constant of the phonon mode near 657 cm^{-1} corresponds to $(A_{1g})_1$ mode of CZFMO decreases, while the damping constant of phonon modes near 205 cm^{-1} corresponds to E(2TO) of the PZTFT increase with Φ as shown in Figure 2. This result indicates that CZFMO experiences a compressive strain, while PZTFT experience tensile strain in the composite. [27]

B. Magnetic Study

Magnetization versus field (M-H) for Φ = 0.1, 0.2, and 0.3 for different temperatures is shown in Figure 3. The M-H data shows that all of the samples have a ferromagnetic response at all measured temperatures, up-to 400 K. The low-temperature saturation moment scales approximately with the CZFMO content, again supporting that the phases are not chemically mixing in the composite and that CZFMO contributes most of the magnetic response. All of the

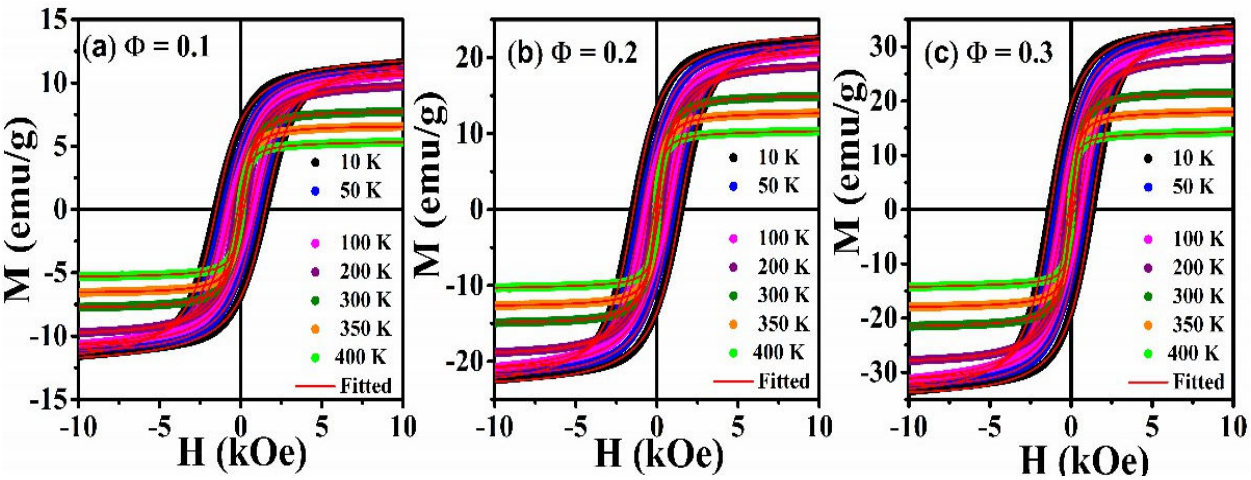

FIGURE 3: The magnetization (M) versus magnetic field (H) curves of (a) Φ = 0.1 (b) Φ = 0.2 and (c) Φ = 0.3, (1- Φ) PZTFT- Φ CZFMO composites at temperature between 10 K and 400 K.

composites show that, at low temperatures, the samples have an appreciable coercivity (>1500 Oe) and remanent magnetization (>0.5 emu/g). Between 10 K and 100 K, with increasing temperature, the coercivity decreases continuously without significant changes in the saturation magnetization, indicating a strong effect from thermally activated reversal. Above 100 K, the coercivity and saturation moment decrease.

Further, in order to extract the ferromagnetic and antiferromagnetic/paramgnetic contribution the M-H loops were fitted using the relation.[27, 31-33]

$$M(H) = \left[\frac{2M_{S(FM)}}{\pi} \tan^{-1} \left\{ \left(\frac{H \pm H_{ci}}{H_{ci}} \right) \tan \frac{\pi M_{r(FM)}}{2M_{S(FM)}} \right\} \right] + \chi H$$

Here, *M(H), M_s, H_{ci}, M_r,* and χ are the measured magnetization as a function of applied magnetic field, saturation magnetization, intrinsic coercivity, remanent magnetization, and magnetic susceptibility, respectively.[27] The 1st term is used to describe ferromagnetic contribution and second term is a linear component used to represent paramagnetic contribution. During the fitting the process, the parameters M_S, H_{ci}, M_r and χ are taken as the input parameters. The approximate value of the parameters M_S, H_{ci} and M_r are taken from the M-H curve where as the approximate value of susceptibility can be taken from the M-T graph. The best fit values of M_S, H_{ci}, M_r and χ are taken from the fitting where we are getting the acceptable value of goodness of fit parameter.

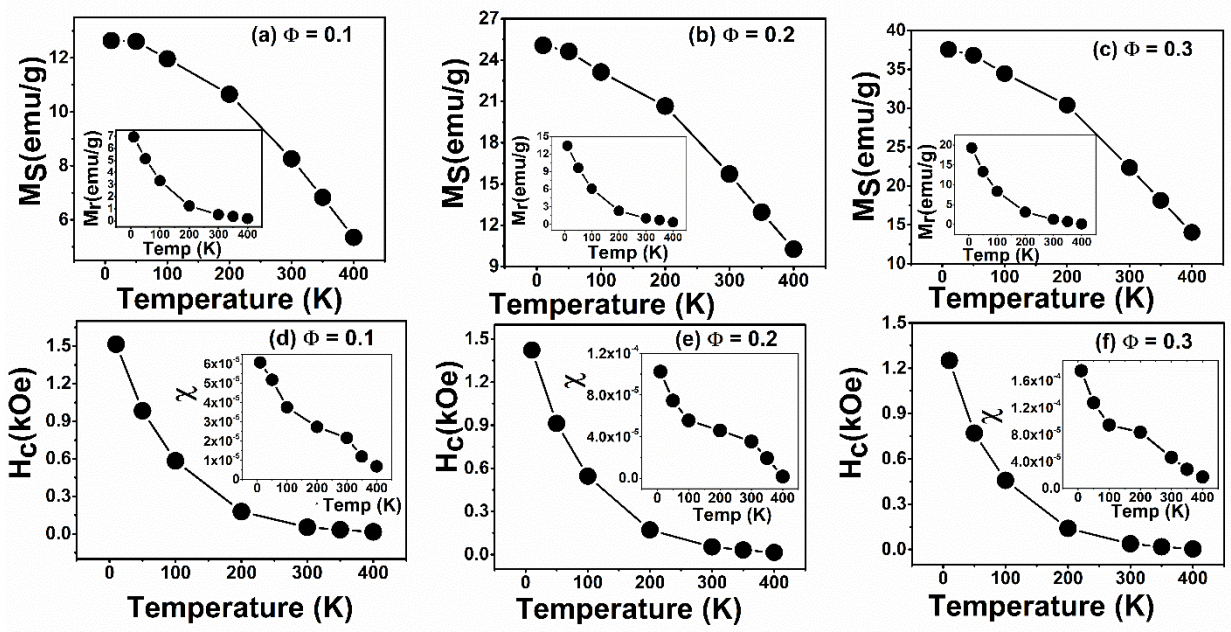

FIGURE 4 The saturation magnetization (M_S) versus temperature (T) curves of (a) Φ = 0.1 (b) Φ = 0.2 and (c) Φ = 0.3, (1- Φ) PZTFT- Φ CZFMO composites versus temperature. Inset shows the

variation of M_r with temperature. (d)-(e) is the variation of H_C with temperature for the composites. Inset (d)-(e) variation of χ with temperature for the composites

The obtained magnetic parameters such as M_s, H_{ci}, M_r for the composites Φ = 0.1, 0.2 an 0.3 are plotted as shown in Figure 4. The M_S and M_r value decreases with increase in temperature where as both of them increase with increase in CZFMO concentration. The low temperature coercivity, H_C, is also shown to decreases with increasing temperature for all composites. The susceptibility (χ) value decreases with rise in temperature for all the compositions (inset Figure 4 (d)-(e)). Increased in the susceptibility value is observed with increase in CZFMO concentration in the composites.

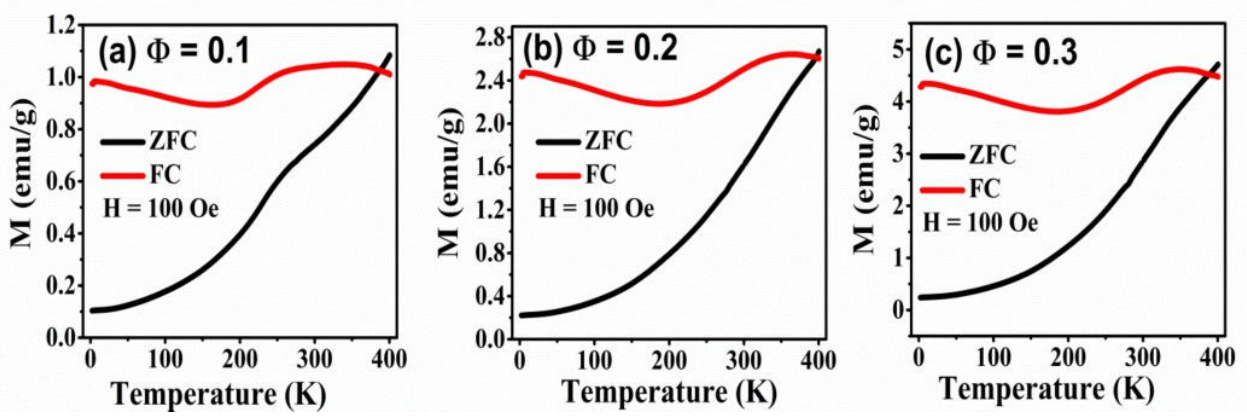

FIGURE 5 ZFC-FC magnetization curves of (a) Φ = 0.1 (b) Φ = 0.2 and (c) Φ = 0.3, (1- Φ) PZTFT- Φ CZFMO composites measured from T = 2K to T = 400 K at H = 100 Oe.

Magnetization versus temperature plots, measured using a ZFC procedure, show the effects of the increasing thermal activation in the increasing magnetic polarization with increasing temperature. Each of the ZFC plots show an inflection in the curves, at 230 K, 315 K and 355 K for Φ = 0.1, 0.2, 0.3, respectively. These inflections indicate that the magnetic anisotropy decreases rapidly at those temperatures, allowing the magnetization to more-easily align with the weak magnetic field.

The FC measurements also show an unusual trend, the most notable of which is a reduction in the magnetization with decreasing temperature, coincident with the inflections in the ZFC curves. Typically, ferro- and ferrimagnetic magnetic materials in a FC measurement show a continuously increasing magnetization with decreasing temperature, following a Curie-Weiss trend. Antiferromagnets on the other hand show an increasing magnetic susceptibility with decreasing temperature, while above their Néel temperature, T_N, which peaks at T_N, then decreases as half of the moments are locked into their antiparallel alignment, orienting one sublattice against the applied magnetic field. Thus, the FC curves, which show such a decrease, likely reflect some antiferromagnetic interaction within the system. The fact that that M-H results do not show an appreciable exchange bias indicates that the ferro and antiferromagnetic phases are either uncoupled, or more likely that the interactions coexist, resulting in a frustrated spin glass. Indeed, CZFMO has been previously reported to have a spin-glass phase.[34, 35]

The ZFC-FC magnetization curve measured in the temperature range 2 K - 400 K at an applied field of H = 100 Oe for Φ = 0.1, 0.2, 0.3 composites are shown in Figure 5(a)-(c) respectively. These measurements show that the irreversibility between ZFC-FC magnetization starts below 350 K for all the composition. The bifurcation between the ZFC magnetization and FC magnetization increases with decreasing temperature. The increase of bifurcation in the low temperature limit suggests highly anisotropic behavior of the composites. The ZFC magnetization curve increases with increase in temperature with a broad anomaly around 230 K for Φ = 0.1, which corresponds to the spin glass transition of CZFMO. [27, 34] It has been reported that CZFMO exhibit a specific magnetic state i.e. semi spin glass state which arises due to the coexistence of longitudinal ferromagnetic component with a transverse spin glass component. [34,35] This type of behavior in spinel is observed due to the addition of weak concentration of nonmagnetic impurities as mention

by Villain.[35] It shifts to 315 K for = 0.2 and 322 K for Φ = 0.3, respectively, though the inflections are more subtle for Φ= 0.2 and 0.3 in the M-T graphs.

C. High Temperature Magnetic Properties

High temperature M-T and M-H measurements are performed on the Φ = 0.2 sample at 315-850 K to capture the ~~magnetic~~ transition temperature and magnetic properties at high temperature ~~(T_C)~~. M-T measurements were conducted in FC configuration, employing a magnetic field of approximately 100 Oe (Figure 6(a)). We observed a systematic decrease in magnetization with increasing temperature, which vanishes beyond ≈532 K~~. indicating T_C~~. Magneto-electric coupling in the composites has been clearly reflected in terms of shifting of the ferroelectric phase transition temperatures of PZTFT phase. However, it is not clearly visible in the M-T plot. So, we have plotted the first order derivative of magnetization with temperature (dM/dT versus T) graph. A broad peak is observed between 450 K which is close to the ferroelectric transition temperature. In Figure 6(b), the M-H loops are presented at various temperatures. At 500 K, the hysteresis loops show the expected sigmoidal response of a ferromagnet, with a narrow coercivity and a saturation field of ≈1 kOe. At higher temperatures, the sigmoidal response disappears, instead taking up the conventional linear response of a paramagnet, confirming the critical temperature identified in the M-T measurements. The magnetic T_C of Φ = 0.2 composite exhibits the magnetic phase transtion temperature above RT at 532±10 K.

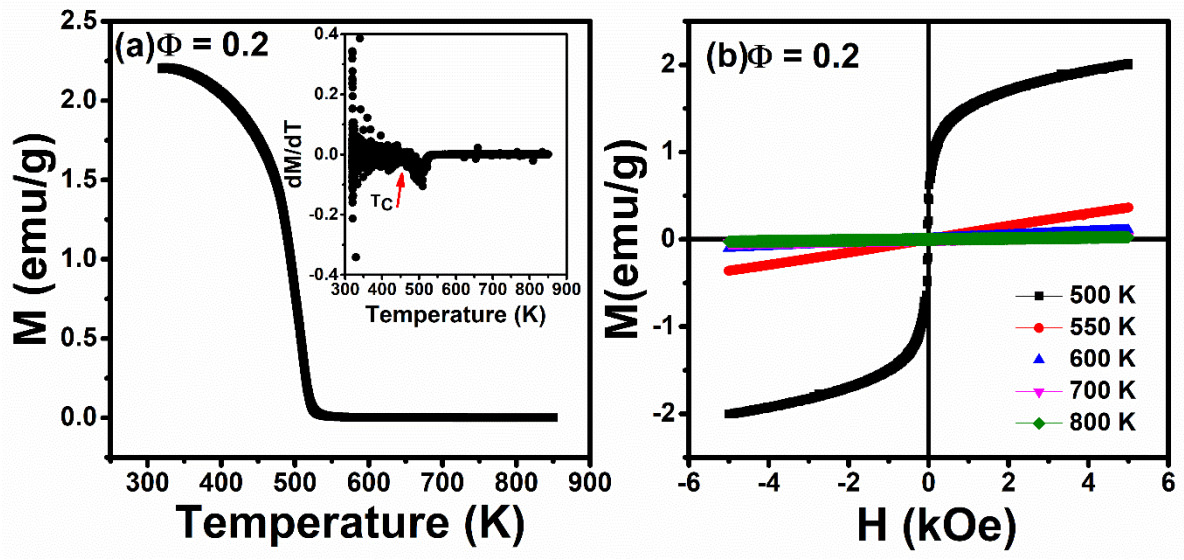

FIGURE 6 Temperature dependence of magnetization measured in FC regimes with an applied static magnetic field of 100 Oe, inset shows the variation of dM/dT versus temperature (b) M-H loops of Φ = 0.2 composite at selected temperatures.

D. Dielectric Studies

To confirm the presence of multiferroic behaviour in these composites above room temperature (RT), we studied the ferroelectric transition behaviour and the effect of CZFMO on the transition temperature of PZTFT phase. The temperature dependent dielectric constants (ε_r) were studied at frequencies of 5 kHz, 10 kHz, 20 kHz, 50 kHz and 100 kHz for Φ = 0, 0.1, 0.2, 0.3 and are shown in Figure 7. For all values of Φ, the ε_r value decreases with increasing frequency suggesting the polar dielectric nature of the systems. [36] The temperature dependence dielectric constant and dielectric loss of CZFMO at different frequencies is reported in our previous work.. From the temperature dependent dielectric constant at different frequencies it was observed that the dielectric constant value increases very slowly up to 415 K, with further increase in temperature a dielectric relaxation peak is observed around 455 K. This dielectric constant peak shifted towards

high temperature with increase in frequency. Similarly, the temperature dependent dielectric loss also shows a frequency dependent relalxation peak around the same temperature range of temperature dependent dielectric constant. The variation of dielectric constant and dielectric loss is in accordance with the reported literature.[26] From the ε_r vs. T plot, it can be observed that the ε_r value increases gradually with increasing temperature and attains a maximum value at 465 K (at 10 kHz) for $\Phi = 0$ (pure PZTFT), which corresponds to ferroelectric orthorhombic to ferroelectric tetragonal phase transitions (T_{o-t}) of PZTFT phase.[9] After $T_{o-t,}$ the ε_r value decreases with further increasing temperature for all frequencies. The dielectric loss value for $\Phi = 0$ increases slowly with increasing temperature and a broad maximum peak is observed around $T_{o-t,}$ which again confirms the ferroelectric (orthorhombic) to ferroelectric (tetragonal) phase transition of PZTFT phase. Overall, a very low value of dielectric loss (tanδ) (≈0.13 at $T_{o-t,}$ 10 kHz) is observed for $\Phi = 0$, which may be advantageous for its use in magneto-electric devices. For the composites $\Phi = 0.1$ and 0.2, the variation of temperature dependent dielectric constant also shows clear ferroelectric-to-ferroelectric transition (due to PZTFT phase) for all frequencies. Above the phase transition temperatures, ≈ 450 K and ≈ 425 K, respectively, the dielectric constant decreases, similar to the $\Phi = 0$ sample, however, the decay is much slower, especially for the low-frequency measurements. The temperature dependent dielectric loss shows a step like increase of dielectric loss value across T_{o-t} for all measured frequencies both for $\Phi = 0.1$ and 0.2. Above the phase transition temperatures the dielectric loss suddenly increases with increasing temperature for all measured frequencies. However for $\Phi = 0.3$ the ε_r vs. T plot shows a relaxation peak (clealy observed at lower frequencies) appearing due to CZFMO phase along with the phase ferroelectric-to-ferroelectric transition (T_{o-t}) due to PZTFT phase. The dielectric relaxation peak shifts to high temperature with increasing frequency. This type of behavior arises due to the electron hopping

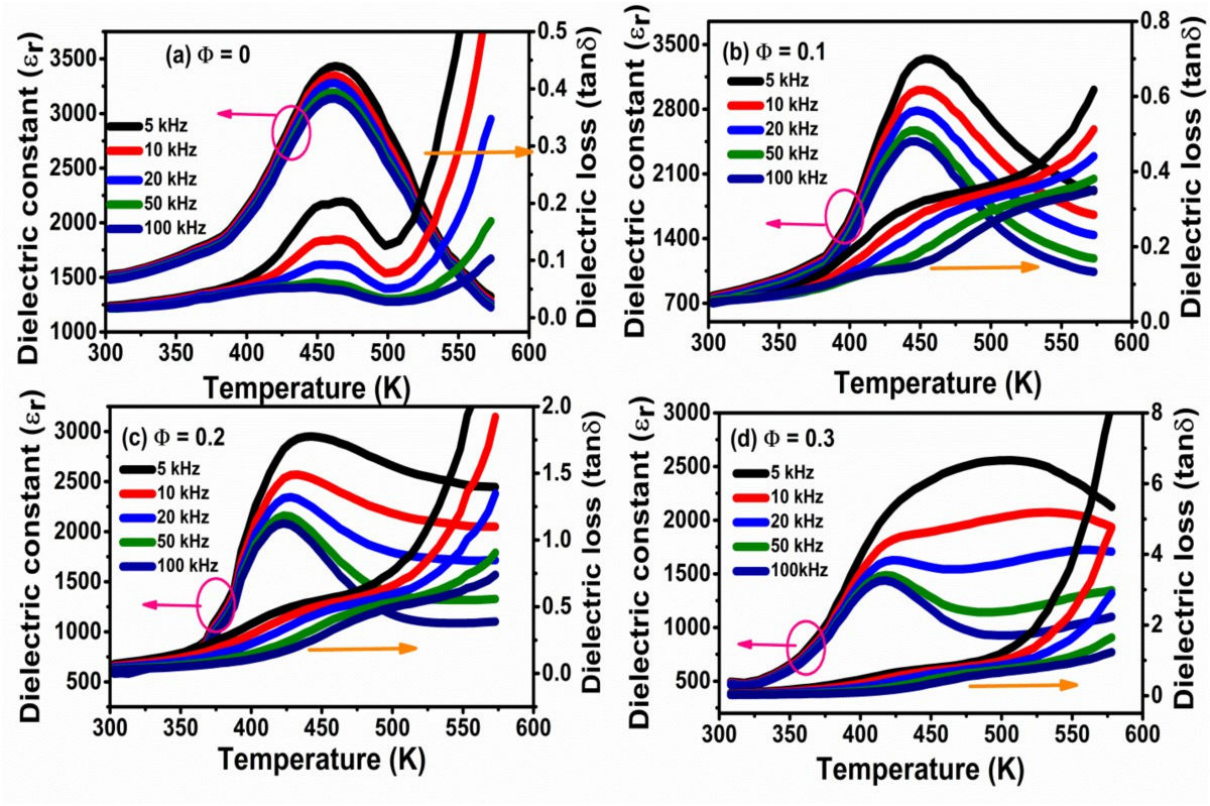

FIGURE 7 The variation of dielectric constant (ε_r) and dielectric loss (tanδ) with temperature for (a) Φ = 0 (b) Φ = 0.1 (c) Φ = 0.2 and (d) Φ = 0.3 for (1- Φ) PZTFT- Φ CZFMO composites at selected frequencies.

between different valance states of Fe (Fe^{2+} and Fe^{3+}) and Mn (Mn^{3+} and Mn^{4+}) ions.[15, 37, 38]. However, the dielectric loss shows a step like increase of dielectric constant around the T_{o-t} phase transition of PZTFT phase for all measured frequencies and there is the sudden increase of dielectric loss around the temperature range of the dielectric relaxation peak. Hence, the dielectric properties in the composite likely arises due to the contribution from both PZTFT ferroelectric-to-

ferroelectric transition (T_{o-t}) from 413 K - 453 K and another relaxation peak due to CZFMO phase around 509 K - 535 K phase again suggesting the composite nature. [26] It has further been observed that the phase transition temperature T_{o-t} of PZTFT phase decreases with the increases in CZFMO concentrations, which may be due to the interaction between the constituent phases. Similar observations have also been reported in the literature for magnetostricitive-ferroelectric composites.[39] The dielectric constant decreases with the addition of CZFMO phase and it is presumably due to the influence of cubic CZFMO phase which has a low dielectric constant value. The increased dielectric loss with the addition of CZFMO is due to the decrease in resistivity of the composite for higher CZFMO concentration.

The diffuse nature of the phase transition also increases with increasing Φ. The diffuse phase transition (DPT) behavior in composites arises due to (i) the compositional heterogeneity model [40, 41] and (ii) octahedral distortion model.[42, 43] According to these two models, the diffuse phase transition behavior is due to the fluctuations of local Curie points. However, Bhat *et.al.*[40], correlated the change in the phase transition temperatures and nature of DPT in multiferroic composites systems based on the Weiss molecular field theory. The reduction of the ferroelectric transition temperature and increase of DPT as observed in the PZTFT-CZFMO composites can be explained by the distribution of local fields and the coupling between the local fields with the dipoles. Hence, the decrease of the transition temperature and diffuseness of the ferroelectric phase arises due to the coupling between the order parameters of the ferroelectric and magnetic phases.[40]

E. Magnetoelectric Properties

The current system is demonstrated to have a magneto-dielectric behavior, e.g. the dielectric response is coupled to the magnetic order and can be changed with the application of a magnetic field. To examine the existence of magnetoelectric behavior at room temperature, we have

measured the capacitance at different magnetic fields i.e. H = 0T, 0.25T, 0.5T, 0.75T, 1T and 1.25T (inset (i) of Figure 8). It has been observed that the dielectric constant decreases with increase in magnetic field (inset (ii) of Figure 8). So change in the dielectric properties by the application of magnetic field suggests the existence of magnetoelectric properties in the systems. However, the exact nature of magnetoelectric coupling, specifically if the coupling is linear (PM), quadratic linear (P^2M or PM^2), or biquadratic (P^2M^2), can be probed from the Ginzburg-Landau theory along with the measured magnetic and magnetoelectric data. The thermodynamic potential ϕ for a ferroelectromagnet can be written as [44, 45]

$$\phi = \phi_0 + \alpha P^2 + \frac{\beta}{2} P^4 - PE + \alpha' P^2 + \frac{\beta'}{2} M^4 - MH + \gamma P^2 M^2 \quad \text{.....(4)}$$

where P = polarization, M = magnetization and α, β, α', β' and γ are coupling coefficients respectively. The term γP^2M^2 is the exchange magnetoelectric interaction and is permitted for any ferroelectromagnet. The difference of relative dielectric constant ($\Delta\varepsilon_r$) is proportional to γP^2M^2 and the sign of γ can be either positive or negative.

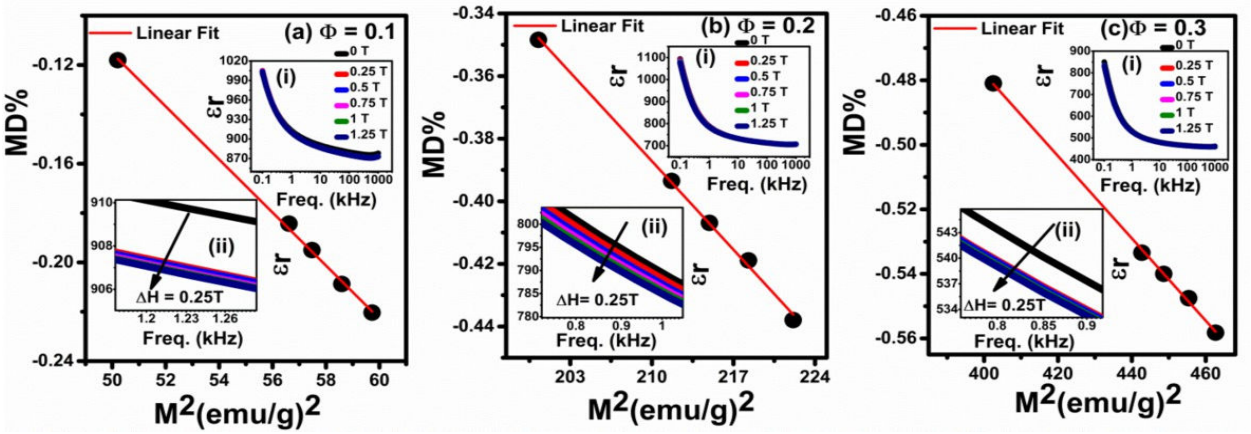

FIGURE 8 The variation of magneto-capacitance versus square of magnetization (M^2) for the composites Φ = (a) 0.1, (b) 0.2, and (c) 0.3. Inset (i) variation of dielectric constant with frequency

at different applied magnetic fields (ii) magnified view of inset (i) to show the effect of magnetic field.

To study the nature of magneto- electric coupling the magnetoapacitance (MD%) versus M^2 plot for the Φ = 0.1, 0.2, 0.3 are shown in Figure 8. The plot is found to be linear in nature, which confirms the existence of biquadratic magneto-electric coupling in the system.[44] Hence, in the current system, this coupling is achieved through strain: an applied magnetic field induces a strain in the magnetic phase through the magnetostrictive effect, which is transferred into the ferroelectric phase, causing a change in the dielectric response.[6]

Inset of Figure 9 (i) shows the variation of magneto-electric coefficient (α) versus DC magnetic field for the (1-Φ) PZTFT-ΦCZFMO (Φ = 0.1, 0.2, 0.3) composites. The magneto-electric coefficient increases, attains a maximum around H_{bias} = 2-3.2 kOe and decreases as the magnetic field is further increased. This magnetic field (H_{bias}) is responsible for the rotation of magnetic domains and is sufficient to cause maximum strain transfer between the piezomagnetic and piezoelectric phases, causing changes the ferroelectric order parameter in the piezoelectric phase. In piezomagnetic-piezoelectric composites, the magnetic field dependence of magnetoelectric coefficient (α) can be studied from magnetic field dependence of magnetostriction coefficient (λ).[46, 47]

The variation of M^2 versus H and dM^2/dH versus H graphs are useful to predict the nature of λ and piezomagnetic coefficient $q = \frac{d\lambda}{dH}$. In order to elucidate the coupling between λ and the piezomagnetic coefficient q, we have plotted M^2 versus H and dM^2/dH versus H graphs as shown in Figure 9. The variation of dM^2/dH versus H is characterized by the appearance of a peak which behaves similar to the magneto-electric coefficient (α) versus DC magnetic field curve. Also, we

have plotted the $\int \alpha_{ME} dH$ versus H and the behavior of the M^2 versus H is qualitatively similar to the $\int \alpha_{ME} dH$ versus H graphs. Further, $\int \alpha_{ME} dH$ versus H graphs give an idea about the λ versus H graphs for PZTFT-CZFMO composites. Therefore we can conclude that the ferroic order parameters such as polarization and magnetization are coupled via mechanical strain. The observed ME coupling in our case could be attributed to various coupling mechanisms. First, when an electric or magnetic field is applied to the composites, the inverse piezoelectric or piezomagnetic effect comes into play. The strain developed in the magnetic phase because of the

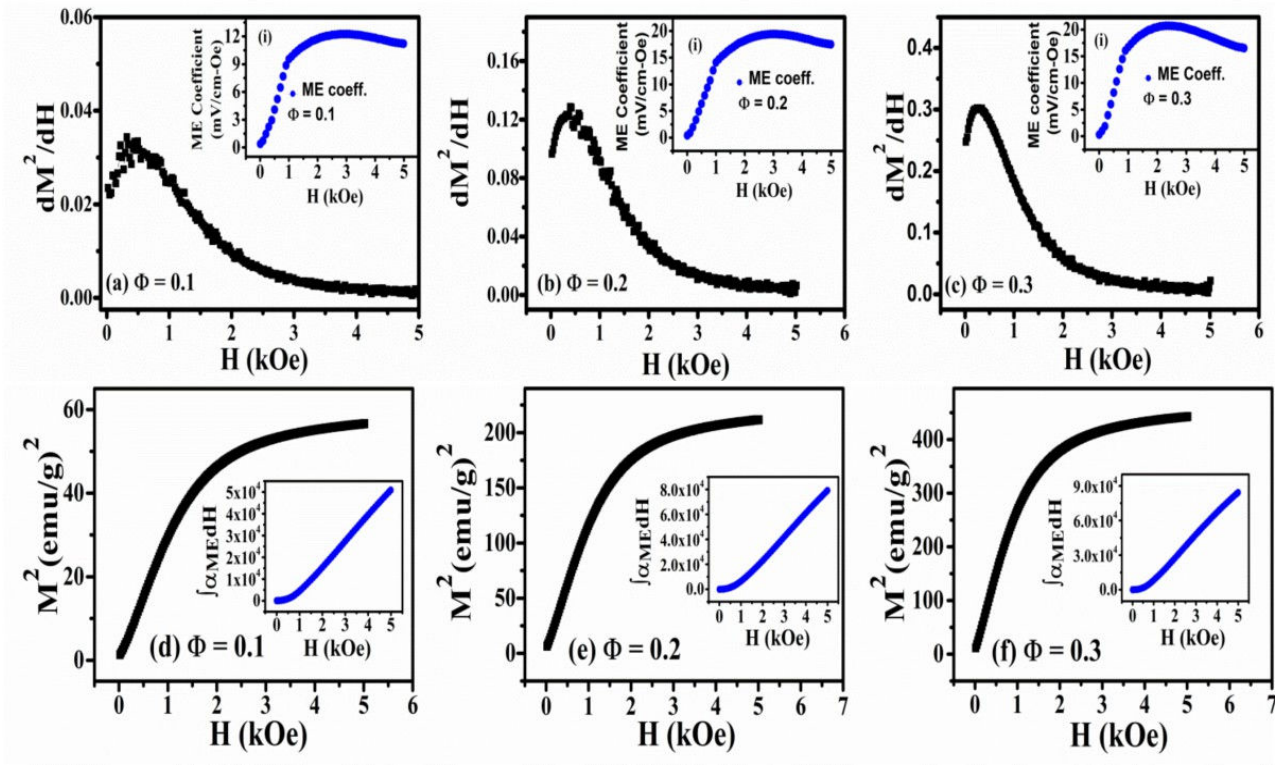

FIGURE 9 (a)-(c) The variation of $\frac{dM^2}{dH}$ versus magnetic field (H), inset ME coefficient versus H for PZTFT-CZFMO composites for Φ = 0.1, 0.2 and 0.3, respectively. Fig.9 (d)–(f) M^2 versus H, inset $\int \alpha_{ME} dH$ versus H graphs for PZTFT-CZFMO composites.

applied magnetic field is transmitted to the ferroelectric phase through the interface.[48-52] Through the piezoelectric effect, the strain alters the polarization and other ferroelectric properties. Secondly, the ME coupling arises from the spin coupling among the magnetic (CZFMO) phase and the multiferroic (PZTFT) phase. This spin coupling induces ionic displacement in both the phases. When switching occurs in the ferroelectric phases, the interatomic distance between the magnetic cations at the interface changes, altering the exchange interaction and leading to the coupling among the order parameters.[48]The third case is the charge coupling between the ferroelectric and magnetic phases. The bound charge at the FE phase brings about a significant modification in charge carrier density within the magnetic phases through charge screening.[48-52]This coupling mechanism circumvents structural distortions and is both reversible and nonvolatile. Charge density plays a fundamental role, as it has the ability to modify the magnetic and electronic properties of these particulate composite through electrostatic doping. This capability allows for precise control of magnetic orderings, electron correlations, orbital states, and transport properties. [48, 52]

IV. CONCLUSIONS

Bi-phasic ME particulate (0-3) composites of PZTFT-CZFMO have been synthesized and various physical properties are investigated. The Raman analysis confirms the composite nature as well as induced strain due to composite fabrication in these samples. The ferroelectric and magnetic phase transitions of these composites are measured from temperature dependent dielectric and magnetic properties and probed to be above RT. The spin glass transition of the CZFMO phase is observed from the M-T graph. The temperature dependent dielectric data also implies the coupled-composite nature of the samples. The biquadratic nature of the magneto-electric coupling behavior is confirmed from the magneto-electric study. The qualitative nature of the piezomagnetic coefficient

is studied from the magnetization versus magnetic field and magnetoelectric coefficient versus magnetic field data. Various mechanisms contributing to the magnetoelectric (ME) coupling are discussed. These composites exhibit magnetic and ferroelectric operational temperature above RT along with strong ME coupling, which makes them well-suited for electronic and memory applications.

ACKNOWLEDGEMENTS

Authors acknowledges UGC DAE, CSR Mumbai Centre (project code: UDCSR/MUM/AO/CSR-M-198) for the financial support and Dr. P. D. Babu for fruitful discussions. Authors would also like to acknowledge Dr. A. K. Singh, Departments of Physics and Astronomy, National Institute of Technology, Rourkela, Odisha 769008, India for providing experimental facility for magneto-dielectric measurement. DAG and WLNCL were supported by DOE Award No. DE-SC0021344.

REFERENCES

1. Eerenstein W, Mathur M. D., Scott J. F. Multiferroic and magnetoelectric materials. *Nature* 2006; **442 :**759-765.
2. Spaldin N. A., Ramesh R. Advances in magnetoelectric multiferroics. *Nat. Mater.* 2019; **18:** 203-212.
3. Khomskii D. Classifying Multiferroics: Mechaisms and Effects. *Physics* 2009, **2**: 20.
4. Nan C.-W., Bichurin M.I, Dong S., Viehland D., Srinivasan G. Multiferroic magnetoelectric composites: Historical perspective, status, and future directions. *J. Appl. Phys.* 2008, **103:** 031101-031135.
5. Jahjah W., Jay J-Ph, Grand Y. L., Fessant A., Prinsloo A. R. E., Sheppard C. J., Dekadjevi D. T., Spenato D. Electrical Manipulation of Magnetic Anisotropy in a

$Fe_{81}Ga_{19}$/$Pb(Mg_{1/3}Nb_{2/3})O_3$-$Pb(Zr_xTi_{1-x})O_3$ Magnetoelectric Multiferroic Composite. *Phys. Rev. Appl.* 2020; **13:**034015.

6. Bhoi K, Mohnaty H. S., Ravikant, Adullah Md. F., Pradhan Dhiren K, Babu S. N., Singh A. K., Vishwakarma P. N., Kumar A., Thomas R., and Pradhan Dillip K. Unravelling the nature of magneto-electric coupling in room temperature multiferroic particulate $(PbFe_{0.5}Nb_{0.5}O_3)$–$(Co_{0.6}Zn_{0.4}Fe_{1.7}Mn_{0.3}O_4)$ composites. *Sci. Rep.* 2021; **11:** 3149.
7. H. Palneedi, V. Annapureddy, S. Priya and J. Ryu, Status and Perspectives of Multiferroic Magnetoelectric Composite Materials and Applications, Actuators 2016, **5:** 9; doi:10.3390/act5010009.
8. Evans D., Schilling A, Kumar A, Sanchez D, Ortega N, Arredondo M, Katiyar R S, Gregg J M, Scott J F, Magnetic switching of ferroelectric domains at room temperature in multiferroic PZTFT. *Nat. Commun. ,* 2013, **4***:* 1534.
9. Sanchez D. A., Ortega N, Kumar A, Roque-Malherbe R, Polanco R, Scott J F, Katiyar R S. Symmetries and multiferroic properties of novel room-temperature magnetoelectrics: Lead iron tantalate – lead zirconate titanate (PFT/PZT). *AIP Advances* 2011; **1:** 042169.
10. Ramana E V, Figueiras F, Graca M P F, Valente M A. Observation of magnetoelectric coupling and local piezoresponse in modified $NaBi_{0.5}Ti_{0.5}O_3$- $BaTiO_3$-$CoFe_2O_4$ lead free composites. *Dalton. Trans.* 2014; **43:** 9934
11. Gupta A, Huang A, Shannigrahi S, Chatterjee R. Improved magnetoelectric coupling in Mn and Zn doped $CoFe_2O_4$ – $PbZr_{0.52}Ti_{0.48}O_3$ particulate composite. *Appl. Phys. Lett.* 2011; **98**: 122901 .
12. Ryu, J Priya S, Uchino K, Kim H E. Magnetoelectric Effect in Composites of Magnetostrictive and Piezoelectric Materials, *J. Electroceram.* 2002: **8:**107-119.

13. Zhang H, Or S W, Chan H L W. Multiferroic properties of $Ni_{0.5}Zn_{0.5}Fe_2O_4$ – $Pb(Zr_{0.53}Ti_{0.47})O_3$ ceramic composites, *J. Appl. Phys.* 2008: **10:** 104109.

14. Pradhan D K, Chowdhury R N P, Nath T K. Magnetoelectric properties of $PbZr_{0.53}Ti_{0.47}O_3$-$Ni_{0.65}Zn_{0.35}Fe_2O_4$ multiferroic nanocomposites. *Appl. Nanosci.*2012; **2** : 261-273

15. Bhoi K, Pradhan D K, Chandrakanta K, Simhachalam N B, . Singh A K, Vishwakarma P N, Kumar A, Rack P D, Pradhan D K. Investigations of room temperature multiferroic and magneto-electric properties of (1-Φ)PZTFT-ΦCZFMO particulate composites. *J. Appl. Phys.* 2023; **133**: 024101.

16. Toulouse J, Jiang F, Svitelskiy O, Chen W, Ye Z.-G. Temperature revolution of the relaxor dynamics in $Pb(Zn_{1/3}Nb_{2/3})O_3$: A critical Raman study. *Phys. Rev. B.* 2005; **72**: 184106.

17. Rahaman M M, Tsukada S, Svirskas S, Banys J, Kojima S. Vibrational dynamics of ferroelectric $K(Ta_{1-x}Nb_xO_3)$ studied by inelastic light scattering. *Ferroelectrics.* 2019; **538**:96–104.

18. Frantti J, Fujioka Y, Puretzky A, Xie Y, Ye Z.-G., Glazer A. A statistical model approximation for perovskite solid solutions: A Raman study of lead-zirconate-titanate single crystal. *J. Appl. Phys.* 2013; **113:** 174104 .

19. Kumari S, Pradhan Dhiren K., Liu S, Rahaman M M, Zhou P, Roccapriore K M, Pradhan Dillip K., Srinivasan G, Li Q, Katiyar Ram S., Rack Philip D., Scott J. F., Kumar A, Room temperature large magnetoelectricity in a transition metal doped ferroelectric perovskites. *Phys. Rev. B*. 2021; **104**: 174415.

20. Sahoo S, Pradhan Dhiren K, Kumari S, Samantaray K S, Singh C, Mishra A, Rahaman M M, Behera B, Kumar A, Thomas R, Rack Philip D, Pradhan Dillip K. Compositional induced structural phase transitions in (1-x) $K_{0.5}Nb_{0.5}O_3$-x$Ba_{0.5}Sr_{0.5}TiO_3$ ferroelectric solid solutions. Sci. Rep.2013; **13**: 19096.

21. Zhu M K, Lu P X, Hou Y D, Song X M, Wang H , Yan H. Analysis of Phase coexistence in Fe_2O_3 doped 0.2PZN-0.8PZT ferroelectrics ceramics by Raman scattering spectra. *J. Am. Ceram. Soc.* 2003; **89**:3739.

22. Siny I G, Tao R, Katiyar R S, Guo R, Bhalla A S. Raman spectroscopy of Mg-Ta order-disorder in $BaMg_{13}Ta_{23}O_3$. *J. Phys. Chem. Solids.* 1998; **59:**181 .

23. Puli V S, Pradhan D K, Pérez W, Katiyar R S, Structure, dielectric tunability, thermal stability and diffuse phase transition behaviour of lead free BZT-BCT ceramic capacitos. *J. Phys. Chem. Solids*. 2013; **74 :**466 .

24. Osada M, Nishida K, Wada S, Okamoto S, Ueno R, Funakubo H, Katoda T. Domain distributions in tetragonal Pb(Zr,Ti)O_3 thin films probed by Raman spectroscopy. *Appl. Phys. Lett.* 2005; **87 :** 232902.

25. Hellwig H. Identification of longitudinal optical modes by hyper-Raman scattering in noncentrosymmetric ceramics. *Appl. Phys. Lett.* 2005; **87**: 051104 .

26. Gupta A, and Chatterjee R, Dielectric and magnetoelectric properties of $BaTiO_3$–$Co_{0.6}Zn_{0.4}Fe_{1.7}Mn_{0.3}O_4$ composite, *J. Eur. Ceram. Soc.* 2013;**33**:1017-1022.

27. Bhoi K, Dash S, Dugu S, Pradhan Dhiren K., Rahaman M M, Simhachalam N B, Singh A K, Vishwakarma P N, Katiyar R S, Pradhan Dillip K. Phase transitions and magneto-electric properties of 70 wt.% Pb($Fe_{0.5}Nb_{0.5}$)O_3-30 wt.% $Co_{0.6}Zn_{0.4}Fe_{1.7}Mn_{0.3}O_4$ multiferroic composites. *J. Appl. Phys. 2021;* **130**:114101 .

28. Chandramohan P, Srinivasan M P, Velmurugan S, Narasimhan S V. Cation distribution and particle size effect on Raman spectrum of $CoFe_2O_4$. *J. Solid State Chem.* 2011; **184** :89.

29. Jacob J, Khadar M A. Investigation of mixed spinel structure of nanostructure nickel ferrite. *J. Appl. Phys.* 2010; **107**:114310.

30. Foerster M, Illiev M, Dix N, Marti X, Barchuk M, Sanchez F, Fontcuberta J. The Poisson ratio in $CoFe_2O_4$ spinel thin films. *Adv. Funct. Mater.* 2012; **22**:4344-4351.

31. Duhalde S., Vignolo M. F., Golmar F., Chiliotte C.and Weissmann M., Appearance of Room Temperature Ferromagnetism in Cu-doped $TiO_{2-\delta}$ films. *Phys. Rev. B.* 2005*;* **72***:* 161313(R).

32. Shah L. R., Zhu H., Wang W. G., Ali B., Zhu T, Fan X, Song Y Q, Wen Q Y, Zhang H W, Shah S I and Xiao J Q, Effect of Zn interstitials on the magnetic and transport properties of bulk Co-doped ZnO, *J. Phys. D. Appl. Phys. 2010;* **43***: 035002.*

33. Kumar P., Shankhwar N., Srinivasan A., and Kar Manoranjan, Oxygen Octahedra Distortion Induced Structural and Magnetic Phase Transitions in $Bi_{1-x}Ca_xFe_{1-x}Mn_xO_3$ ceramics, *J. Appl. Phys. 2015;* **117***:194103.*

34. Gupta A, Tandon R P, Shinde A B, Krishna P S R, Chatterjee R. Nagative spontaneous magnetization and semi-spin glass magnetic order in mixed spinel $Co_{0.6}Zn_{0.4}Fe_{1.7}Mn_{0.3}O_4$.*J. Appl. Phys.* 2015; **118**: 133902.

35. Villian J, Insulating Spin Glasses. *Z. Phys. B.* 1979; **33**:31.

36. Barick B K, Mishra K K, Arora A K, Chaudhary R N P, Pradhan Dillip K. Impedance and Raman spectroscopic studies of $(Na_{0.5}Bi_{0.5})TiO_3$. *J. Phys. D: Appl. Phys.* 2011; **44**:355402.

37. Kim H Chang, Myung Y, Cho J Yong, Kim H S, Park S-H, Park J, Kim J-Y, Kim B, Electronic Structure of Vertically Aligned Mn-Doped $CoFe_2O_4$ Nanowires and Their Application as Humidity Sensors and Photodetectors, *J. Phys. Chem. C* 2009; **113**: 7085-7090.

38. Krieble K, Schaeffer T, Paulsen J. A, Ring A. P., Lo C C H, Snyder J. E., Mossbauer Spectroscopy Investigation of Mn-substituted Co-ferrite ($CoMn_xFe_{2x}O_4$), *J. Appl. Phys.* 2005; **97**, 10F101.

39. Ciomaga C Elena, Neagu A. Maria, Pop M. Valentin, Airimioaei M., Tascu S, Schileo G, Gallasi C, Mitoseriu L, Ferroelectric and dielectric properties of ferrite-ferroelectric ceramic composites. *J. Appl. Phys.2013***; 113**: 074103 .

40. Bhat V V, Umarji A M, Shenoy V B, Waghmare U V. Diffuse ferroelectric phase transitions in Pb-substituted $PbFe_{1/2}Nb_{1/2}O_3$. *Phys. Rev. B.* 2005; **72**:014104 .

41. Smolensky G. Ferroelectric with diffuse phase transitions. *Ferroelectrics* 1984; **53**: 129–135 .

42. Bokov A A, *Ferroelectrics.* Recent advances in diffuse ferroelectric phase transitions. 1992; **131**:49.

43. Bokov V A, Shpak L A, and Rayevsky I P. Diffuse phase transition in $Pb(Fe_{0.5}Nb_{0.5}O_3)$-based solid solutions. *J. Phys. Chem. Solids. 1993;* ***54:*** 495 .

44. Adhlakha N, Yadav K L, Singh R. Effect of $BatiO_3$ addition on structural, multiferroic and magnetodielectric properties of $0.3CoFe_2O_4$-$0.7BiFeO_3$ ceramics. *Smart. Mater.Struct.* 2014; **23:** 105024 .

45. Kimura T, Kawamoto S, Yamada I, Azuma M, Takano M, Tokura Y. Magnetocapacitance effect in multiferroic $BiMnO_3$. *Phys. Rev. B.* 2003; **67**: 180401.

46. Yan Y, Zhou Y, and Priya S. Giant self-biased magnetoelectric coupling in co-fired textured layered composites. *Appl. Phys. Lett.* 2013;**102**:052907 .

47. Wu R, Kurumovic A, Gao X, Yun C, Vickers M E, Wang H, Cho S, and MacManus-Driscoll J L. Design of a vertical composite thin film system with ultra low leakage to yield large converse magnetoelectric effect. *Appl. Mater. Interfaces.* 2018; **10:** 18237.

48. Pradhan D K, Kumari S, and Rack P D. Magnetoelectric composites: applications, coupling mechanisms and future directions. *Nanomaterials.* 2020; **10**:2072 .

49. Ma J, Hu J, Li Z, Nan C W. Recent progress in multiferroic magnetoelectric composites from bulk to thin films. *Adv. Mater. 2011;* **23:** 1062-1087 .

50. Pradhan D K, Mohanty H S, Kumari S, Bhoi K, Tang N, Ravikant, Rahaman M M, Pradhan D K, Kumar A, Gilbert D A and Rack P D.Ferroic phase transition and magnetoelectric coupling in cobalt doped $BaTiO_3$. *J. Mater. Chem. C.*, 2021; 9:12694-12711

51. Vaz C A F, and Staub U. Artificial multiferroic heterostructures. *J. Mater. Chem. C.* 2013; **1**:6731-6742 .

52. Kumari S, Pradhan D K, Das P T, Ortega N, . Pradhan K, Kumar K, Scott J F Katiyar R S, Evidence of strong magneto-dielectric coupling and enhanced electrical insulation at room temperature in Nd and Mn co-doped bismuth ferrite. *J. Appl. Phys.* 2017; **122:** 144102.